Symmetric Double-Well Potential Model and Its Application to Vibronic Spectra: Studies of Inversion Modes of Ammonia and Nitrogen-Vacancy Defect Centers in Diamond†

Chih-Kai Lin,*,‡,§ Huan-Cheng Chang,‡ and S. H. Lin‡

Institute of Atomic and Molecular Sciences, Academia Sinica, P.O. Box 23-166, Taipei, Taiwan 10617, Republic of China, and Taiwan International Graduate Program, Department of Chemistry, National Tsing Hua University, Hsinchu, Taiwan 30013, Republic of China

Received: May 18, 2007; In Final Form: July 31, 2007

In this paper, we have studied the vibronic transitions between two symmetric double-well potentials by proposing a model Hamiltonian consisting of a harmonic oscillator and a parturition described by a Gaussian function that leads to a double minima potential with a barrier between the two energy minima. Making use of the contour integral form of Hermite polynomials, we present a new formula that can calculate Franck−Condon factors of the system rigorously. The simulated vibronic spectra of ammonia and the negatively charged nitrogen-vacancy center in diamond are presented as an application of the formula.

I. Introduction

The vibrational modes of molecules, in general, are defined at the potential energy surface minimum and well-described by harmonic oscillators near the equilibrium. Some modes, however, may have double or multiple potential minima, such as inversion, ring-puckering, large-amplitude bending, and torsional vibrations.[1] A single harmonic oscillator is unable to describe these types of motion, and a number of approaches have been proposed to construct double- or multiple-well potential surfaces. Prominent approaches include the quadratic potential perturbed by a Gaussian function barrier,[2,3] the quartic−quadratic potential,[4] the hyperbolic secant functions,[5] and the linear combination of cosine functions,[1] etc. Each of them has its own advantage—for instance, the cosine potential is suitable for the multiple minima case, the hyperbolic secant potential permits an exact solution to the Schrödinger equation,[5] and the quadratic−Gaussian potential and the quartic−quadratic potential fit most accurately the vibrational levels of symmetric double minima.[1,2,6]

In this work, we selected the quadratic function with a Gaussian function barrier as the template for the symmetric double-well potential. Taking harmonic oscillator wavefunctions as the basis set, a new numerical method is presented to evaluate the coupled matrix elements of the Gaussian function using the contour integral representation of Hermite polynomials. The Schrödinger equation was solved variationally to determine the vibrational levels, and the corresponding wavefunctions were obtained as a linear combination of the harmonic oscillator wavefunctions. This was followed by the calculation of Franck−Condon factors between two double-well potentials to investigate vibronic transitions, in which overlap integrals of wavefunctions between these two different-shaped potentials and matrix elements of vibrational coordinates were computed. We finally simulated absorption and emission vibronic spectra to compare with experimental data.

Two systems have been chosen to demonstrate the feasibility of this approach. The first is the $\tilde{A}-\tilde{X}$ transition of ammonia, which shows pronounced vibrational progressions involving the inversion mode (ν_2) in both absorption[7−13] and fluorescence spectra[14−16] where up to 10 and to 4 ν_2 quanta, respectively, have been observed. Our simple one-dimensional formula can reproduce the absorption spectrum satisfactorily. The second is the negatively charged nitrogen-vacancy defect center in diamond, denoted as $(N-V)^-$. The center, with a C_{3v} symmetry, is created by electron bombardment of diamond containing dispersed nitrogen atoms, followed by thermal annealing at elevated temperatures.[17−20] It exhibits a sharp zero-phonon line (ZPL) at 637 nm (1.945 eV) at liquid nitrogen or lower temperature, accompanied with a broad vibronic sideband. The ZPL becomes less obvious when the temperature rises.[21−27] Our model could readily depict the nitrogen tunneling motion in this center,[18,28,29] fitting well both absorption and fluorescence spectra.

II. Theories

1. Energy Levels and Wavefunctions of the Symmetric Double-Well Potential. We first took the harmonic oscillator potential as the unperturbed system and the corresponding wavefunctions as the basis set. A Gaussian-type barrier was then introduced,

$$V(Q) = \frac{1}{2}\omega_0{}^2Q^2 + A\exp(-\alpha Q^2) \tag{1}$$

where ω_0 ($=h\nu_0$) is the unperturbed harmonic oscillator angular frequency and Q is the mass-weighted coordinate. The top of the barrier locates at $Q = 0$ with $V(0) = A$; the equilibrium positions $\pm Q_m$ (bottoms of the potential double-well) satisfy

$$Q_m{}^2 = \frac{1}{\alpha}\ln\left(\frac{2\alpha A}{\omega_0{}^2}\right) \equiv \frac{\rho}{\alpha} \tag{2}$$

with the potential

$$V(Q_m) = \frac{A}{e^{\rho}}(\rho + 1) \tag{3}$$

In eq 2, we adopted the potential-shape parameter ρ introduced

† Part of the "Sheng Hsien Lin Festschrift".

* Corresponding author. E-mail: ethene@gate.sinica.edu.tw. Fax: 886-2-23620200.

‡ Academia Sinica.

§ National Tsing Hua University.

10.1021/jp073838i CCC: $37.00
Published on Web 08/29/2007

by Coon et al.[6] for convenience. Further defining the barrier height $B \equiv V(0) - V(Q_m)$ leads to

$$V(0) = A = \frac{Be^{\rho}}{e^{\rho} - \rho - 1} \tag{4a}$$

and

$$V(Q_m) = \frac{B(\rho + 1)}{e^{\rho} - \rho - 1} \tag{4b}$$

For this system, the Schrödinger equation is written as

$$\hat{H}\Psi = (\hat{H}_0 + \hat{H}')\Psi = \left[-\frac{\hbar^2}{2}\frac{\partial^2}{\partial Q^2} + \frac{1}{2}\omega_0{}^2Q^2 + A\exp(-\alpha Q^2)\right]\Psi = E\Psi \tag{5}$$

where $\hat{H}'$ refers to the Gaussian barrier as a perturbation. We took the trial function Θ as a normalized linear combination of the unperturbed harmonic oscillator wavefunctions,

$$\Theta = \sum_{n=0}^{\infty} c_n \psi_n \tag{6}$$

and solved eq 5 variationally. The secular equation was deduced as

$$|H_{mn} - \delta_{mn}W| = 0 \tag{7}$$

or

$$\left|H'_{mn} + \delta_{mn}\left(n + \frac{1}{2} - W\right)\right| = 0 \tag{8}$$

where W is the variational energy, m and n are the numbering of the unperturbed harmonic oscillator wavefunctions, and the Gaussian-coupled matrix elements are defined as

$$H_{mn} = \langle\psi_m|\hat{H}|\psi_n\rangle$$

$$H'_{mn} = \langle\psi_m|\hat{H}'|\psi_n\rangle = \int_{-\infty}^{\infty}\psi_m A\exp(-\alpha Q^2)\psi_n\,dQ \tag{9}$$

Instead of using the recursion formulas,[6] we performed the integration of eq 9 by using the contour integral representation of Hermite polynomials (see section A of the Supporting Information for details). The results are

$$H'_{mn} = A\left(\frac{m!n!}{2^{m+n}}\right)^{1/2}\sqrt{\frac{\beta}{\alpha+\beta}}\cdot\sum_{l=0}^{\infty}\Pr(m-l-1)\cdot \Pr(n-l-1)\cdot\frac{1}{l!}\left(\frac{2\beta}{\alpha+\beta}\right)^{l}\frac{\left(-\frac{\alpha}{\alpha+\beta}\right)^{(m+n-2l)/2}}{\left(\frac{m-l}{2}\right)!\left(\frac{n-l}{2}\right)!} \tag{10a}$$

for even $m + n$, and

$$H'_{mn} = 0 \tag{10b}$$

for odd $m + n$. Here $\Pr(x)$ is the parity-checking function, defined as

$$\Pr(x) = \begin{cases} 0, & x \text{ even} \\ 1, & x \text{ odd} \end{cases} \tag{11}$$

which ensures that both $m - l$ and $n - l$ are even in eq 10a.

The equations can be readily solved numerically. In principle, infinite terms in the linear combinations of harmonic oscillator wavefunctions should be considered, but in practice, 32 terms will be sufficient to give vibrational energies of interest with five digit precision. These energies (W's in eq 8) and coefficients of the linear combinations (c_n's in eq 6) were subsequently obtained for any given pair of (ρ, B) parameters.

2. Franck−Condon Factors of Distorted Harmonic Oscillators. To evaluate the intensity of the vibronic transition involving a single vibrational mode between two symmetric double-well potentials, we started with the nuclear wavefunctions represented by the linear combination of harmonic oscillator wavefunctions as

$$\Theta_{a\upsilon} = \sum_{n=0}^{\infty} c_{a\upsilon,n}\psi_n$$

$$\Theta_{b\upsilon'} = \sum_{m=0}^{\infty} c_{b\upsilon',m}\psi'_m \tag{12}$$

where aυ refers to the electronic state a with vibrational quantum υ, and bυ' to the electronic state b with vibrational quantum υ'. Notice that the two double-well potentials are represented here by two sets of harmonic oscillator wavefunctions with two different frequencies but of the same origin, i.e., distorted harmonic oscillators (without displacement). The intensity of the transition between these two states is then proportional to[30−33]

$$|\vec{\mu}_{b\upsilon',a\upsilon}|^2 = |\langle\Psi_{b\upsilon'}|\vec{\mu}|\Psi_{a\upsilon}\rangle|^2 = |\langle\Phi_b\Theta_{b\upsilon'}|\vec{\mu}|\Phi_a\Theta_{a\upsilon}\rangle|^2 \approx |\langle\Theta_{b\upsilon'}|\vec{\mu}_{ba}|\Theta_{a\upsilon}\rangle|^2 \tag{13}$$

where the Born−Oppenheimer adiabatic approximation is applied to separate the wavefunction into the nuclear part Θ and the electronic part Φ. The electronic transition moment $\vec{\mu}_{ba}$ is defined as $\vec{\mu}_{ba} \equiv \langle\Phi_b|\vec{\mu}|\Phi_a\rangle$ and can be expanded as

$$\vec{\mu}_{ba}(Q) = \vec{\mu}_{ba}(0) + \sum_i\left(\frac{\partial\vec{\mu}_{ba}}{\partial Q_i}\right)_0 Q_i + \frac{1}{2}\sum_i\sum_j\left(\frac{\partial^2\vec{\mu}_{ba}}{\partial Q_i\partial Q_j}\right)_0 Q_iQ_j + \ldots \tag{14}$$

When the first term in eq 14 dominates, as the usual case of symmetry-allowed transitions, eq 13 could be approximated as

$$|\vec{\mu}_{b\upsilon',a\upsilon}|^2 \approx |\vec{\mu}_{ba}(0)|^2|\langle\Theta_{b\upsilon'}|\Theta_{a\upsilon}\rangle|^2 \tag{15}$$

The term $|\langle\Theta_{b\upsilon'}|\Theta_{a\upsilon}\rangle|^2$ is the Franck−Condon factor for symmetry-allowed transition, and in our derivation it becomes

$$|\langle\Theta_{b\upsilon}|\Theta_{a\upsilon'}\rangle|^2 = \left|\langle\sum_{m=0}^{\infty}c_{b\upsilon',m}\psi'_m\left|\sum_{n=0}^{\infty}c_{a\upsilon,n}\psi_n\right\rangle\right|^2 = \left|\sum_{m=0}^{\infty}\sum_{n=0}^{\infty}c_{b\upsilon',m}c_{a\upsilon,n}\langle\psi'_m|\psi_n\rangle\right|^2 = \left|\sum_{m=0}^{\infty}\sum_{n=0}^{\infty}c_{b\upsilon',m}c_{a\upsilon,n}S_{mn}\right|^2 \tag{16}$$

where

$$S_{mn} \equiv \langle\psi'_m|\psi_n\rangle \tag{17}$$

is the overlap integral of distorted harmonic oscillator wavefunctions. The direct integration of S_{mn} resembles that of H'_{mn} and yields (see section B of the Supporting Information for details)

$$S_{mn} = \left(\frac{m!n!}{2^{m+n}} \cdot \frac{2\sqrt{\beta\beta'}}{\beta+\beta'}\right)^{1/2} \sum_{l=0}^{\infty} \Pr(m-l-1)\cdot \Pr(n-l-1)\cdot \frac{(-1)^{(m-l)/2}}{l!}\left(\frac{4\sqrt{\beta\beta'}}{\beta+\beta'}\right)^{l} \frac{\left(\frac{\beta-\beta'}{\beta+\beta'}\right)^{(m+n-2l)/2}}{\left(\frac{m-l}{2}\right)!\left(\frac{n-l}{2}\right)!} \quad (18a)$$

for even $m + n$, and

$$S_{mn} = 0 \quad (18b)$$

for odd $m + n$. The relationship between the vibrational frequencies of the two harmonic oscillators can be denoted by $\omega' = f\omega$ or $\beta' = f\beta$, where f is a proportional factor. Equation 18a then becomes

$$S_{mn} = \left(\frac{m!n!}{2^{m+n}} \cdot \frac{2\sqrt{f}}{1+f}\right)^{1/2} \sum_{l=0}^{\infty} \Pr(m-l-1)\cdot \Pr(n-l-1)\cdot \frac{(-1)^{(m-l)/2}}{l!}\left(\frac{4\sqrt{f}}{1+f}\right)^{l} \frac{\left(\frac{1-f}{1+f}\right)^{(m+n-2l)/2}}{\left(\frac{m-l}{2}\right)!\left(\frac{n-l}{2}\right)!} \quad (19)$$

In the case that $\vec{\mu}_{ba}(0)$ is zero (symmetry-forbidden) or small compared with the higher-order terms in eq 14, eq 15 can be rewritten, assuming that only a single vibrational mode is involved, as

$$\begin{aligned} |\vec{\mu}_{b\nu',a\nu}|^2 &= \left\{\langle\Theta_{b\nu'}|\vec{\mu}_{ba}(0)|\Theta_{a\nu}\rangle + \left\langle\Theta_{b\nu'}\left|\left(\frac{\partial\vec{\mu}_{ba}}{\partial Q}\right)_0 Q\right|\Theta_{a\nu}\right\rangle + \frac{1}{2}\left\langle\Theta_{b\nu'}\left|\left(\frac{\partial^2\vec{\mu}_{ba}}{\partial Q^2}\right)_0 Q^2\right|\Theta_{a\nu}\right\rangle + \ldots\right\}^2 \\ &= |\vec{\mu}_{ba}(0)|^2|\langle\Theta_{b\nu'}|\Theta_{a\nu}\rangle|^2 + \left(\frac{\partial\vec{\mu}_{ba}}{\partial Q}\right)_0^2 |\langle\Theta_{b\nu'}|Q|\Theta_{a\nu}\rangle|^2 + \vec{\mu}_{ba}(0)\left(\frac{\partial^2\vec{\mu}_{ba}}{\partial Q^2}\right)_0 \langle\Theta_{b\nu'}|\Theta_{a\nu}\rangle\langle\Theta_{b\nu'}|Q^2|\Theta_{a\nu}\rangle + \ldots \end{aligned} \quad (20)$$

Defining the coupling of wavefunctions through Q and Q^2 as

$$\begin{aligned} S^{(1)}_{mn} &\equiv \langle\Theta_{b\nu'}|Q|\Theta_{a\nu}\rangle \\ S^{(2)}_{mn} &\equiv \langle\Theta_{b\nu'}|Q^2|\Theta_{a\nu}\rangle \end{aligned} \quad (21)$$

we derived that (see section C of the Supporting Information for details)

$$S^{(1)}_{mn} = \frac{1}{\sqrt{\beta}(1+f)}\left(\frac{m!n!}{2^{m+n}}\cdot\frac{2\sqrt{f}}{1+f}\right)^{1/2} \sum_{l=0}^{\infty}\frac{1}{l!}\left(\frac{4\sqrt{f}}{1+f}\right)^{l}\left(\frac{1-f}{1+f}\right)^{(m+n-2l-1)/2} \times 2\left\{\Pr(m-l-1)\cdot\Pr(n-l)\cdot\frac{(-1)^{(m-l)/2}}{\left(\frac{m-l}{2}\right)!\left(\frac{n-l-1}{2}\right)!} + \Pr(m-l)\cdot\Pr(n-l-1)\cdot\frac{(-1)^{(m-l-1)/2}\sqrt{f}}{\left(\frac{m-l-1}{2}\right)!\left(\frac{n-l}{2}\right)!}\right\} \quad (22)$$

and

$$S^{(2)}_{mn} = \frac{1}{\beta(1+f)}S_{mn} + \frac{1}{\beta(1+f)^2}\left(\frac{m!n!}{2^{m+n}}\cdot\frac{2\sqrt{f}}{1+f}\right)^{1/2} \sum_{l=0}^{\infty}\frac{1}{l!}\left(\frac{4\sqrt{f}}{1+f}\right)^{l}\left(\frac{1-f}{1+f}\right)^{(m+n-2l-2)/2} \times \left\{4\cdot\Pr(m-l-1)\cdot\Pr(n-l-1)\cdot\left[\frac{(-1)^{(m-l)/2}}{\left(\frac{m-l}{2}\right)!\left(\frac{n-l-2}{2}\right)!} + \frac{(-1)^{(m-l-2)/2}\cdot f}{\left(\frac{m-l-2}{2}\right)!\left(\frac{n-l}{2}\right)!}\right] + 8\cdot\Pr(m-l)\cdot\Pr(n-l)\cdot\frac{(-1)^{(m-l-1)/2}\cdot\sqrt{f}}{\left(\frac{m-l-1}{2}\right)!\left(\frac{n-l-1}{2}\right)!}\right\} \quad (23)$$

3. Absorption and Photoluminescence Spectra. In the Born−Oppenheimer adiabatic approximation, the absorption coefficient $\alpha(\omega)$ for the vibronic transition from electronic state a to b with vibrational quanta ν and ν', respectively, can be expressed as[30−33]

$$\alpha(\omega) = \frac{4\pi^2\omega}{3\hbar c}\sum_{\nu}\sum_{\nu'}P_{a\nu}|\langle\Theta_{b\nu'}|\vec{\mu}_{ba}|\Theta_{a\nu}\rangle|^2 D(\omega_{b\nu',a\nu}-\omega) \quad (24)$$

where $P_{a\nu}$ denotes the Boltzmann factor of the initial state, $\vec{\mu}_{ba}$ is the electronic dipole moment, and $D(\Delta\omega)$ is the Lorentzian function. Similarly, the photoluminescence spectra can be described by

$$I(\omega) = \frac{4\omega^3}{3\hbar c^3 A_{b\to a}}\sum_{\nu}\sum_{\nu'}P_{b\nu'}|\langle\Theta_{a\nu}|\vec{\mu}_{ba}|\Theta_{b\nu'}\rangle|^2 D(\omega_{b\nu',a\nu}-\omega) \quad (25)$$

where $A_{b\to a}$ denotes the radiative rate constant of the transition from state b to a. In the Lorentzian function,

$$D(\omega_{b\nu',a\nu}-\omega) = \frac{1}{\pi}\frac{\gamma_{b\nu',a\nu}}{\gamma_{b\nu',a\nu}^2 + (\omega_{b\nu',a\nu}-\omega)^2} \quad (26)$$

TABLE 1: Fitting Parameters of the Symmetric Double-Well Potential of the Inversion Mode (ν_2) of Ammonia

	NH_3		ND_3	
parameters	ground state, $\tilde{X}$ (double-well)	excited state, $\tilde{A}$ (nearly harmonic)	ground state, $\tilde{X}$ (double-well)	excited state, $\tilde{A}$ (nearly harmonic)
ρ^a	0.60	0.60	0.60	0.60
$B\ (h\nu_0)^b$	2.086	0.046	2.679	0.003
$B\ (cm^{-1})^b$	2032	42.8	1984	2.04
$\nu_0\ (cm^{-1})^c$	974.2	931.1	740.5	678.3
$G(0^+)\ (cm^{-1})^d$	513.2	345.9	394.0	333.5
$A\ (h\nu_0)^e$	17.11	0.377	21.98	0.024
$A\ (cm^{-1})^e$	16670	351.3	16274	16.7
$\alpha\ (2\pi\nu_0/\hbar)^e$	0.0532	2.41	0.0415	37.0

[a] Symmetric double-well potential-shape parameter defined in eq 2. [b] Barrier-height parameter used in eq 4. [c] Unperturbed harmonic oscillator frequency. [d] Energy difference between the first vibrational level and the bottom of the well; zero-point energy at the ground state. [e] Barrier parameters defined in eq 1.

TABLE 2: Experimental and Calculated Vibrational Levels (in cm^{-1}) of the ν_2 Mode in the Ground and the First Electronically Excited States of NH_3

$\tilde{X}$ state			$\tilde{A}$ state		
v	exp[a]	calc	v'	exp[b]	calc
0^+	0.00	0.00	0	46222	46222[c]
0^-	0.79	0.83	1	47057	47023
1^+	932.4	932.4	2	47964	47964
1^-	968.2	967.8	3	48869	48875
2^+	1602	1603.0	4	49783	49803
2^-	1882.2	1882.8	5	50730	50729
3^+	2383.5	2385.0	6	51656	51657
3^-	2895.5	2891.7	7	52543	52585
4^+	3442	3453.2	8	53496	53514
4^-		4047.4	9	54454	54443

[a] From ref 36. [b] From ref 12. [c] Experimental band origin adopted.

TABLE 3: Experimental and Calculated Vibrational Levels (in cm^{-1}) of the ν_2 Mode in the Ground and the First Electronically Excited States of ND_3

$\tilde{X}$ state			$\tilde{A}$ state		
v	exp[a]	calc	v'	exp[b]	calc
0^+	0.000	0.000	0	46701	46701[c]
0^-	0.053	0.058	1	47369	47373
1^+	745.7	745.7	2	48052	48052
1^-	749.4	749.4	3	48697	48729
2^+	1359	1361.2	4	49375	49407
2^-	1429	1432.3	5	50062	50086
3^+	1830	1831.9	6	50748	50764
3^-	2106.6	2111.6	7	51451	51442
4^+	2482	2485.5	8	52162	52120
4^-	2876	2876.5	9	52874	52799

[a] From ref 36. [b] From ref 12. [c] Experimental band origin adopted.

$\gamma_{b\upsilon',a\upsilon}$ denotes the dephasing (or damping) constant, which is related to the lifetime τ's of the two states,

$$\gamma_{b\upsilon',a\upsilon} = \frac{1}{2}\left(\frac{1}{\tau_{a\upsilon}} + \frac{1}{\tau_{b\upsilon'}}\right) \tag{27}$$

In the case of excitation from the ground state with $\upsilon = 0$, $\gamma_{b\upsilon',a\upsilon}$ depends only on the lifetime of the final state $b\upsilon'$, which in turn depends mainly on the vibrational relaxation process. Because the vibrational relaxation in a harmonic oscillator occurs via the linear coupling through vibrational coordinates, the relaxation rate is then proportional to

$$|\langle\Theta_{b\upsilon'}|Q|\Theta_{b(\upsilon'-1)}\rangle|^2 = \frac{\upsilon'}{2\beta} \tag{28}$$

Thus $\gamma_{b\upsilon',a\upsilon}$ is linearly proportional to υ'.

III. Results and Discussion

1. Inversion Mode of Ammonia. The inversion mode, ν_2, of ammonia is a well-known vibrational motion with a symmetric double-well potential. The equilibrium configuration of NH_3 at the ground state ($\tilde{X}$) is pyramidal, and the molecule can flip over its mirror position (with a barrier of $\sim$2020 cm^{-1}) when the umbrella vibrational motion is highly excited.[3,6,34,35] The first electronically excited state ($\tilde{A}$), on the other hand, has a planar geometry at equilibrium.[8,34,35]

We have carried out calculations as described in section II.1 to search for proper ρ and B parameters that construct the double-well potential and fit well with experimentally observed vibrational frequencies. These two parameters and related constants are listed in Table 1, and a comparison of the calculated and experimental vibrational levels for both the ground and the excited states is given in Tables 2 and 3 for NH_3 and ND_3, respectively.[12,36]

In the $\tilde{A} \leftarrow \tilde{X}$ transition of ammonia, the absorption spectrum consists mainly of the progression in the ν_2 mode. It has been noticed that in the case of NH_3, the intensities of the vibronic bands show some anomalies. At room temperature, the peaks split due to rotation-vibration coupling.[12,37,38] When the molecule was cooled down by supersonic expansion with argon, the splitting disappears but some even−odd intensity alternations occur.[12,13,39] For example, the transition to $\upsilon' = 4$ has an anomalous intensity, which is lower than its adjacent transitions, $\upsilon' = 3$ and 5. This incongruity was suggested as a result of the selection rule on nuclear permutation symmetry for protons at low temperatures.[13,38] Such an effect was less obvious in the absorption spectra of ND_3. Because our model does not take into account any rotations or nuclear spins, we took ND_3 to test our formulation.

TABLE 4: Calculated Matrix Elements of $\langle\Theta_{b\upsilon'}|\Theta_{a\upsilon}\rangle$ for the $\tilde{A}-\tilde{X}$ Transition of ND_3

	υ'									
υ	0	1	2	3	4	5	6	7	8	9
0^+	0.0688	0.0000	0.2690	0.0000	0.4873	0.0000	0.5749	0.0000	0.4871	0.0000
0^-	0.0000	0.1570	0.0000	0.3861	0.0000	0.5539	0.0000	0.5499	0.0000	0.4011
1^+	0.2616	0.0000	0.5258	0.0000	0.4262	0.0000	0.0095	0.0000	−0.3641	0.0000
1^-	0.0000	0.4176	0.0000	0.5346	0.0000	0.2427	0.0000	−0.2038	0.0000	−0.4510

TABLE 5: Calculated Matrix Elements of $\langle\Theta_{b\upsilon'}|Q^2|\Theta_{a\upsilon}\rangle$ for the $\tilde{A}-\tilde{X}$ Transition of ND_3

	υ'									
υ	0	1	2	3	4	5	6	7	8	9
0^+	0.2453	0.0000	1.7090	0.0000	4.6218	0.0000	7.5266	0.0000	8.4589	0.0000
0^-	0.0000	0.7733	0.0000	3.0373	0.0000	6.2138	0.0000	8.3202	0.0000	7.9590
1^+	0.5490	0.0000	2.4431	0.0000	3.1166	0.0000	−0.1457	0.0000	−5.7025	0.0000
1^-	0.0000	1.3986	0.0000	3.1934	0.0000	2.0415	0.0000	−2.8987	0.0000	−7.9791

TABLE 6: Experimental and Calculated Relative Band Intensities of the ν_2 Progression in the $\tilde{A} \leftarrow \tilde{X}$ Absorption of ND_3

		calculated[b] with $\vec{\mu}'_{ab}$ =						
υ'	exp[a,b]	0.00	0.05	0.10	0.15	0.20	0.25	0.30
0	c	1.4	0.9	0.6	0.5	0.4	0.4	0.3
1	c	7.5	5.0	3.8	3.1	2.6	2.3	2.1
2	16	22	16	13	11	9.5	8.6	8.0
3	28	47	35	29	26	24	22	21
4	51	75	61	53	48	45	43	41
5	74	99	85	78	73	70	68	67
6	92	108	100	96	93	91	90	89
7	100	100	100	100	100	100	100	100
8	96	80	86	90	93	94	96	97
9	90	55	64	70	74	77	79	81
10	77	32	42	48	52	55	57	59

[a] From ref 12. [b] Relative band areas with respect to the $\upsilon' = 7$ band. [c] Feature too weak to be estimated.

According to the Condon approximation as shown in eq 15, the intensities of the vibronic transitions are proportional to the Franck−Condon factors, $|\langle\Theta_{b\upsilon'}|\Theta_{a\upsilon}\rangle|^2$. However, in the $\tilde{A} \leftarrow \tilde{X}$ absorption transition of ND_3, the highest peak occurs at $\upsilon' = 7$, whereas the calculated Franck−Condon factors show a maximum at $\upsilon' = 6$. Durmaz et al.[40] suggested that higher order terms in the expansion of $\vec{\mu}_{ba}(Q)$ (cf. eq 14) must be taken into account. Following this suggestion, we considered the vibronic coupling through Q^2 and rewrote eq 20 as

$$|\vec{\mu}_{b\upsilon',a\upsilon}|^2 \approx \left\{\langle\Theta_{b\upsilon'}|\vec{\mu}_{ba}(0)|\Theta_{a\upsilon}\rangle + \frac{1}{2}\left\langle\Theta_{b\upsilon'}\left|\left(\frac{\partial^2\vec{\mu}_{ba}}{\partial Q^2}\right)_0 Q^2\right|\Theta_{a\upsilon}\right\rangle\right\}^2$$

$$= |\vec{\mu}_{ba}(0)|^2\left\{\langle\Theta_{b\upsilon'}|\Theta_{a\upsilon}\rangle + \frac{1}{2\vec{\mu}_{ba}(0)}\left(\frac{\partial^2\vec{\mu}_{ba}}{\partial Q^2}\right)_0\langle\Theta_{b\upsilon'}|Q^2|\Theta_{a\upsilon}\rangle\right\}^2 \quad (29)$$

A short list of the calculated matrix elements, with the application of the overlap integrals introduced in section II.2, is given in Tables 4 and 5 for the zeroth-order and second-order terms, respectively. Because the term $\langle\Theta_{b\upsilon'}|Q^2|\Theta_{a\upsilon}\rangle$ has a maximum at $\upsilon' = 8$, we may take the second-order correction term $\vec{\mu}'_{ab} \equiv (\partial^2\vec{\mu}_{ba}/\partial Q^2)_0/\vec{\mu}_{ba}(0)$ as an adjustable parameter to match the experimental result. The relative band intensities are listed in Table 6 as a function of $\vec{\mu}'_{ab}$, and we found that the best fitting was given by $\vec{\mu}'_{ab} = 0.20$.

Figure 1 shows the simulated absorption spectra after convolution of the calculated stick spectrum with a Lorentzian profile for each peak. The Lorentzian width of each transition was assumed, for simplicity, to be proportional to the vibrational energy (cf. eq 28), and 8 cm^{-1} was taken for the $\upsilon' = 1^+$ peak. The calculated vibronic bands can quantitatively reproduce the experimental data up to $\upsilon' = 7$. Discrepancies appear for higher vibrational quanta, including band position shift attributed to anharmonicity,[3,13,32] band shape inconsistency because the widths do not increase monotonically,[13,38] and band intensity variance caused by coupling with the ν_1 symmetric stretching mode.[41−44]

TABLE 7: Experimental and Calculated Relative Band Intensities of the ν_2 Progression in the $\tilde{A} \rightarrow \tilde{X}$ Emission of ND_3

		calculated[b] with $\vec{\mu}'_{ab}$ =						
υ	exp[a,b]	0.00	0.05	0.10	0.15	0.20	0.25	0.30
0^+	0.5[c]	1.2	1.3	1.5	1.7	1.8	2.0	2.1
1^+	19[c]	16	17	18	19	20	21	22
2^+	100	100	100	100	100	100	100	100
3^+	112	91	88	84	81	78	75	73
4^+	26	15	13	12	11	10	9.0	8.2
5^+		1.7	1.4	1.2	1.0	0.8	0.7	0.6

[a] From ref 15. [b] Relative band areas with respect to the $\upsilon = 2^+$ band. [c] Estimated in the original paper.

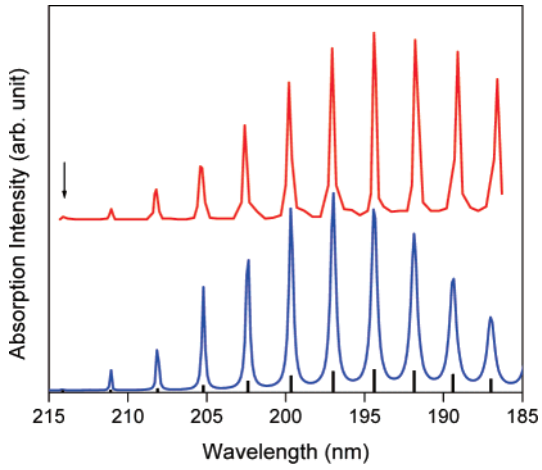

Figure 1. Comparison of experimental and calculated absorption spectra of the $\tilde{A} \leftarrow \tilde{X}$ absorption transition of ND_3 with the vibrational progression in the ν_2 mode. The upper trace is the experimental spectrum adopted from ref 12 whereas the lower trace is the simulated spectrum calculated according to eq 24. The vertical bars indicate the corrected Franck−Condon factors (eq 29) multiplied by the transition energies and by the Boltzmann factors at $T = 150$ K. The Lorentzian width of each transition was assumed proportional to the vibrational energy, and 8 cm^{-1} was taken for the $\upsilon' = 1^+$ peak.

We have carried out similar calculations to reproduce the fluorescence intensities of the $\tilde{A} \rightarrow \tilde{X}$ transition involving the inversion mode. The relative intensities are listed in Table 7, along with the simulated fluorescence spectrum in Figure 2. Note that we have considered only transitions related to ν_2 in this calculation and neglected the additional progression involving the ν_1 mode to the longer-wavelength region.[14−16] Although the experimental spectrum shows the highest fluorescence peak at $\upsilon = 3^+$, our model gives a maximum at $\upsilon = 2^+$, a result similar to that of Rosmus et al.[42] using an unmodified ab initio surface. Despite those minor factors not considered in the simple model, our formulas concerning the symmetric double-well potential are valid to a substantial level in describing the vibronic transitions of the ammonia molecule involving the inversion

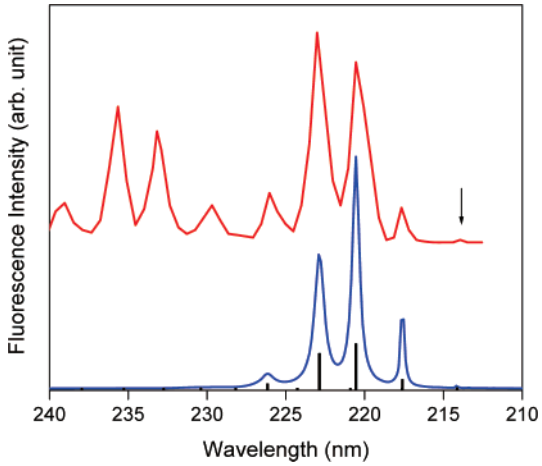

Figure 2. Comparison of experimental and calculated fluorescence spectra of the $\tilde{A} \rightarrow \tilde{X}$ emission transition of ND_3 with the vibrational progression in the ν_2 mode. The upper trace is the experimental spectrum adopted from ref 15 whereas the lower trace is the simulated spectrum calculated according to eq 25. The vertical bars indicate the corrected Franck−Condon factors (eq 29) multiplied by the cubic of transition energies and by the Boltzmann factors at $T = 150$ K. The Lorentzian width of 25 cm^{-1} was taken for the $v = 1^+$ peak. Note that only the progression of the ν_2 mode was presented in this simulation.

mode. This promises the capability of the formulation applying to systems that have a similar behavior.

2. Nitrogen-Vacancy Defect Center of Diamond. Among hundreds of kinds of defect centers found in diamonds, the negatively charged nitrogen-vacancy center [denoted $(N-V)^-$] is of high interest for several advantages concerning its photoluminescence. It is a red fluorescence chromophore with quantum yield near unity[45] and is much more stable than common dye molecules under continuous irradiation.[23] Its ZPL locates at 637 nm (1.945 eV) and the vibronic band extends to near-infrared, which has little overlap with emission from any biomolecule.[27] On the basis of these optical properties and the low cytotoxicity of diamond itself, the N−V center in nanodiamonds could act as an excellent fluorescent biomarker that can be fed into living cells and easily detected under a microscope.[23,27,46]

The N−V centers usually emerge after a certain manufacturing procedure of type Ib diamonds. These nitrogen-containing diamonds (typically 100 ppm dispersed nitrogen atoms) are first subjected to high-energy particle (electron, neutron, proton, etc.) irradiation (∼2 MeV), followed by high-temperature annealing (∼900 °C).[17−20] In this procedure vacancies are created by bombardment and then migrate to the neighbor sites of substitutional nitrogen atoms. Each nitrogen-vacancy pair thus locates along a C_{3v} axis, the nitrogen bonded with three carbon atoms and the vacancy enclosed by other three. From experiments such as uniaxial stress,[18] electron paramagnetic resonance,[47,48] photon echo,[49] etc. the ground state of the defect center is determined as ^3A and the excited state ^3E, with a ^1A state located slightly lower than the ^3E state.[22,25,26,45] The lifetime of the ^3E state was found to be ∼13 ns.[49,50] Under intense irradiation the center may lose its charge to yield $(N-V)^0$, which has the ZPL at 575 nm (2.156 eV).[24,25,51,52]

The absorption and emission spectra concerning the N−V center were first reported in early 1970s.[17] Davies and Hamer have then made a thorough examination of the spectra at liquid nitrogen temperature with higher resolution and found some interesting fine structures.[18] In both absorption and fluorescence spectra, pronounced ZPLs at 1.945 eV due to the $^3A-^3E$ transition of $(N-V)^-$ can be easily assigned. In addition, the

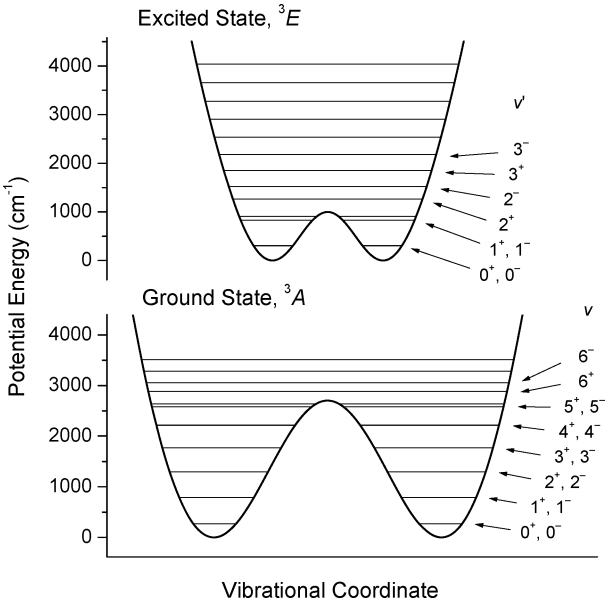

Figure 3. Parameter-fitted symmetric double-well potentials and vibrational levels referring to the ground and the excited states of the diamond $(N-V)^-$ center. Note that the well of the excited state is much shallower than that of the ground state, resulting in an absorption doublet at the transitions to the $v' = 1^+$ and 1^- levels but an emission singlet at the transitions to the degenerate $v = 1^+$ and 1^- levels.

vibronic bands in these two spectra are nearly mirror images of each other, if some minor features related to other defect centers are ignored. It was noticed, however, that there exists an absorption doublet at 2.01 and 2.02 eV that have not been resolved previously whereas the corresponding fluorescence peak is just a singlet. The authors have recommended a double-well potential model based on displaced dual harmonic oscillators to account for this discrepancy.[18] In this model, the nitrogen atom was proposed to tunnel through a barrier to the vacancy site (i.e., position exchange of the nitrogen atom and the vacancy) in a symmetric double-well potential, and the barrier height at the excited state is much lower than that at the ground state, resulting in a small splitting in the $v' = 1^+$ and 1^- levels at the excited state while the $v = 1^+$ and 1^- levels remain degenerate at the ground state (see Figure 3).

Following this pioneering work, Kilin et al.[28,29] have employed double-cosine functions to model the double-well potential. In the present work, we applied the strategy described in section II to refine the analysis. Parameters that fit positions of the experimentally observed absorption doublet and fluorescence peaks are listed in Table 8. The sets of (ρ, B) that fit best with the experimental values are (0.90, 6.70) for the ground state and (1.20, 2.38) for the excited state. As shown in Figure 3, the potential well of the excited state is so shallow that only 4 vibrational levels ($v' = 0^+$, 0^-, 1^+, and 1^-) reside under the barrier. In contrast, the ground state barrier is higher so that levels up to $v = 5^-$ are enclosed in the double-well.

Using these parameters, we reconstructed both absorption and fluorescence spectra of the $(N-V)^-$ center, which are shown in Figures 4 and 5a. The vibronic bands pertinent to the nitrogen tunneling mode are severely broadened due to effective coupling of the electronic transition with phonons, especially at large vibrational quanta. The band broadening prevents resolution of any fine structures, except the ZPLs and the transitions to $v' = 1^+$ and 1^- in the absorption spectrum and to $v = 1-3$ in the fluorescence spectrum. Our simulated absorption spectrum, if neglecting all minor peaks due to other defect centers (e.g., at

TABLE 8: Fitting Parameters of the Symmetric Double-Well Potential Involving the Nitrogen Tunneling Mode of the $(N-V)^-$ Center in Diamond

parameters	ground state, ^3A fit 1[a]	fit 2[b]	fit 3[c]	excited state, ^3E
ρ[d]	0.90	0.90	0.90	1.20
B ($h\nu_0$)[e]	6.70	6.20	5.80	2.38
B (cm^{-1})[e]	2706	2512	2357	1000
ν_0 (cm^{-1})[f]	403.9	405.2	406.3	420.0
$G(0^+)$ (cm^{-1})[g]	267.2	267.6	268.1	305.4
A ($h\nu_0$)[h]	14170	11041	10360	2963
A (cm^{-1})[h]	0.0335	0.0451	0.0482	0.235

[a] Based on data from ref 18. [b] Based on data from ref 17. [c] Based on data from ref 23. [d] Symmetric double-well potential-shape parameter defined in eq 2. [e] Barrier-height parameter used in eq 4. [f] Unperturbed harmonic oscillator frequency. [g] Energy difference between the first vibrational level and the bottom of the well; zero-point energy at the ground state. [h] Barrier parameters defined in eq 1.

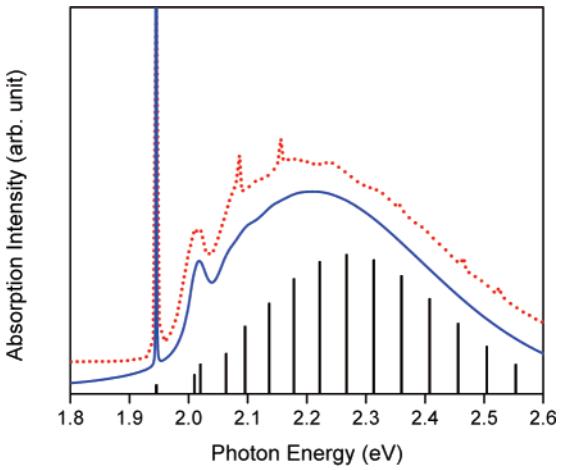

Figure 4. Comparison of experimental and calculated absorption spectra of the diamond $(N-V)^-$ center. The upper trace is the experimental spectrum adopted from ref 18 with baseline subtraction whereas the lower trace is the simulated spectrum. The two traces are slightly displaced in purpose for a clearer presentation. The vertical bars depict calculated Franck−Condon factors multiplied by the transition energies and by the Boltzmann factors at $T = 77$ K, which were converted to the simulated spectrum by convolution with Lorentzian profiles. The Lorentzian width of each transition was assumed to be proportional to the vibrational energy, and 120 cm^{-1} was taken for the $\upsilon' = 1^+$ peak.

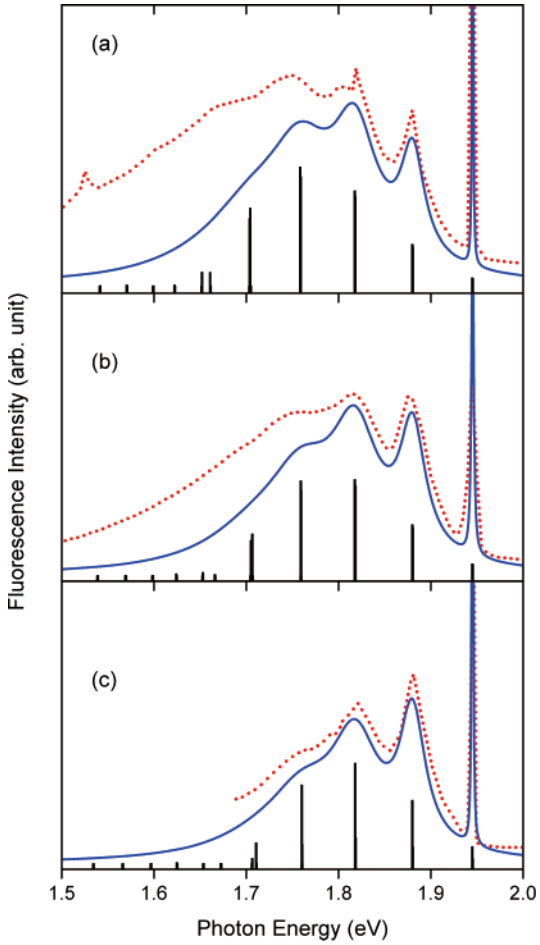

Figure 5. Comparison of experimental and calculated fluorescence spectra of the diamond $(N-V)^-$ center. In each frame the upper trace is the experimental data, the lower trace is the simulated spectrum, and the vertical bars represent the Franck−Condon factors multiplied by the cubic of transition energies and by the Boltzmann factors. Note that pairs of traces are slightly displaced from each other for a better visualization. The experimental spectra are adopted from (a) ref 18, (b) ref 17, and (c) ref 25. The fitting parameters are shown in Table 8. The Lorentzian profiles used in convolution of simulated spectra were assumed to have widths proportional to the vibrational energies, and a value of 120 cm^{-1} was taken for the $\upsilon = 1^+$ peak.

2.086 and 2.156 eV),[53] is in reasonable agreement with the experimental data (after baseline subtraction).[18]

The fluorescence spectrum, however, presents a large inconsistency between calculated and experimental results. The large tail (low-energy region) in the experimental spectrum might have contributions from other luminescent defect centers, for example, the 1.819 eV center.[18] We also found that, by comparing experimental results from different reports, the highest fluorescent peak usually occurs at $\upsilon = 1$ or 2 together with a rapidly dropping tail,[21−27] rather than at $\upsilon = 3$ with a large tail.[18] It should be addressed that there are always variations between experimental spectra from different samples because of various manufacturing processes, defect lattice environments, and photoexcitation conditions, etc.[22,25,27] It has been demonstrated by Kilin et al. that the spectral shapes and hence the fitting parameters (of their model) would be very different from each other.[29] We therefore launched a systematic exploration on how the parameters affect the spectral shape and tried to fit other experimental spectra. A general trend showed that lowering the barrier-height parameter B or increasing the potential-shape parameter ρ of the ground state causes the highest fluorescent peak shifting toward $\upsilon = 1$. In fitting the emission spectrum reported by Clark and Norris at liquid nitrogen temperature,[17] a slightly different set of parameters was adopted for the ground state. Figure 5b shows the experimental and simulated results; the discrepancy in the tail still exists. A better match was obtained in fitting the one reported by Manson et al. at 5 K with lower irradiation intensity,[25] as shown in Figure 5c. All the fitting parameters and related properties are listed in Table 8. We noticed that, in addition to the possible background contributed by other centers, the discrepancy could be a result of the fact that the detection efficiency varies at different wavelengths but the reported emission intensity might not be normalized with respect to the spectral response. Should this be calibrated, the fitting is expected to improve.

In a recent discussion on the electronic model of the N−V center,[54] the authors queried if the double-well potential model is conclusive, for the evidence till now is only the absorption doublet. The well depths were found around 2500 cm^{-1} for the ground state and 1000 cm^{-1} for the excited state in fitting the model. For such shallow wells the tunneling splitting in vibrational levels that yields two transition frequencies (or sets

of frequencies) is expected, but this is not yet observed in experiments. We found in our modeling that the splitting in the ZPL, i.e., the energy difference between $v = 0^+$ and $v' = 0^+$ and between $v = 0^-$ and $v' = 0^-$ transitions, is about $4-5$ cm^{-1} ($0.5-0.6$ meV). This feature would thus be completely embedded in the inhomogeneous broadening, typically 30 cm^{-1}, of the ZPL in a bulk system due to a large strain variation.[22] Even when a single defect center was detected, the fluorescence excitation spectra presented the full width at half-maximum around 5 cm^{-1} (0.6 meV),[45] which could hardly tell whether the splitting exists. This indeed remains an issue that higher resolution in experimental spectra is required to examine the validity of the symmetric double-well potential model applying to the diamond nitrogen-vacancy defect center. Ab initio calculations can be expected to assist in describing possible vibronic transitions in this chromophore.

IV. Conclusions

In this study, we have treated the vibrational motion of an oscillator in a symmetric double-well based on a harmonic oscillator potential perturbed by a Gaussian function barrier. Matrix elements of the perturbed harmonic oscillator wavefunctions were evaluated using a new numerical approach, yielding accurate vibrational energy levels and corresponding wavefunctions. To investigate vibronic transitions involving such vibrational modes, Franck−Condon factors and higher-order vibronic terms were calculated by taking into account direct and coordinate-coupled wavefunction overlap integrals between distorted potentials.

We have then applied the formulas to the inversion mode of ammonia and the nitrogen-tunneling mode of the nitrogen-vacancy defect center in diamond. The potential-shape parameters were first determined, followed by simulation of absorption and fluorescence spectra. In the $\tilde{A} \leftarrow \tilde{X}$ absorption spectrum of ND_3, satisfactory fitting up to $v' = 7$ of the progression of the ν_2 mode has been obtained. Good agreements between experimental and calculated spectra were also achieved for the $^3A-{}^3E$ transition of the diamond $(N-V)^-$ center. These two examples demonstrate the capability and reliability of this simple formulation, and further applications of the modeling to other molecular systems can be anticipated.

Supporting Information Available: Detailed derivations of the Gaussian-coupled matrix elements, the overlap integrals of distorted harmonic oscillators, and the coordinate-coupled overlap integrals. This material is available free of charge via the Internet at http://pubs.acs.org.

References and Notes

(1) Hollas, J. M. *High Resolution Spectroscopy*; Butterworth: London, 1982.
(2) Chan, S. I.; Zinn, J.; Fernandez, J.; Gwinn, W. D. *J. Chem. Phys.* **1960**, *33*, 1643.
(3) Swalen, J. D.; Ibers, J. A. *J. Chem. Phys.* **1962**, *36*, 1914.
(4) Laane, J.; Lord, R. C. *J. Chem. Phys.* **1967**, *47*, 4941.
(5) Manning, M. F. *J. Chem. Phys.* **1935**, *3*, 136.
(6) Coon, J. B.; Naugle, N. W.; McKenzie, R. D. *J. Mol. Spectrosc.* **1966**, *20*, 107.
(7) Tannenbaum, E.; Coffin, E. M.; Harrison, A. J. *J. Chem. Phys.* **1953**, *21*, 311.
(8) Walsh, A. D.; Warsop, P. A. *Trans. Faraday Soc.* **1961**, *57*, 345.
(9) Douglas, A. E. *Discuss. Faraday Soc.* **1963**, *35*, 158.
(10) Lassettre, E. N.; Skerbele, A.; Dillon, M. A.; Ross, K. J. *J. Chem. Phys.* **1968**, *48*, 5066.
(11) Rabalais, J. W.; Karlsson, L.; Werme, L. O.; Bergmark, T.; Siegbahn, K. *J. Chem. Phys.* **1973**, *58*, 3370.
(12) Vaida, V.; Hess, W.; Roebber, J. L. *J. Phys. Chem.* **1984**, *88*, 3397.
(13) Vaida, V.; McCarthy, M. I.; Engelking, P. C.; Rosmus, P.; Werner, H. J.; Botschwina, P. *J. Chem. Phys.* **1987**, *86*, 6669.
(14) Koda, S.; Hackett, P. A.; Back, R. A. *Chem. Phys. Lett.* **1974**, *28*, 532.
(15) Gregory, T. A.; Lipsky, S. *J. Chem. Phys.* **1976**, *65*, 5469.
(16) Tang, S. L.; Abramson, E. H.; Imre, D. G. *J. Phys. Chem.* **1991**, *95*, 4969.
(17) Clark, C. D.; Norris, C. A. *J. Phys. C* **1971**, *4*, 2223.
(18) Davies, G.; Hamer, M. F. *Proc. R. Soc. London A* **1976**, *348*, 285.
(19) Davies, G.; Lawson, S. C.; Collins, A. T.; Mainwood, A.; Sharp, S. J. *Phys. Rev. B* **1992**, *46*, 13157.
(20) Collins, A. T.; Connor, A.; Ly, C.-H.; Shareef, A.; Spear, P. M. *J. Appl. Phys.* **2005**, *97*, 083517.
(21) Gruber, A.; Dräbenstedt, A.; Tietz, C.; Fleury, L.; Wrachtrup, J.; von Borczyskowski, C. *Science* **1997**, *276*, 2012.
(22) Jelezko, F.; Tietz, C.; Gruber, A.; Popa, I.; Nizovtsev, A.; Kilin, S.; Wrachtrup, J. *Single Mol.* **2001**, *2*, 255.
(23) Yu, S.-J.; Kang, M.-W.; Chang, H.-C.; Chen, K.-M.; Yu, Y.-C. *J. Am. Soc. Chem.* **2005**, *127*, 17604.
(24) Manson, N. B.; Harrison, J. P. *Diamond Relat. Mater.* **2005**, *14*, 1705.
(25) Manson, N. B.; Harrison, J. P.; Sellars, M. J. *Phys. Rev. B* **2006**, *74*, 104303.
(26) Jelezko, F.; Wrachtrup, J. *Phys. Status Solidi A* **2006**, *203*, 3207.
(27) Fu, C.-C.; Lee, H.-Y.; Chen, K.; Lim, T.-S.; Wu, H.-Y.; Lin, P.-K.; Wei, P.-K.; Tsao, P.-H.; Chang, H.-C.; Fann, W. *Proc. Natl. Acad. Sci. U.S.A.* **2007**, *104*, 727.
(28) Kilin, S. Y.; Nizovtsev, A. P.; Maevskaya, T. M.; Gruber, A.; Dräbenstedt, A.; Wrachtrup, J.; von Borczyskowski, C. *Opt. Spectrosc.* **1999**, *87*, 624.
(29) Kilin, S. Y.; Nizovtsev, A. P.; Maevskaya, T. M.; Dräbenstedt, A.; Wrachtrup, J. *J. Lumin.* **2000**, *86*, 201.
(30) Liang, K. K.; Chang, R.; Hayashi, M.; Lin, S. H. *Principle of Molecular Spectroscopy and Photochemistry*; National Chung-Hsing University Press: Taichung, 2001.
(31) Eyring, H.; Lin, S. H.; Lin, S. M. *Basic Chemical Kinetics*; Wiley-Interscience: New York, 1981; Chapters 7 and 8.
(32) Lin, S. H.; Fujimura, Y.; Neusser, H. J.; Schlag, E. W. *Multiphoton Spectroscopy of Molecules*; Academic Press: New York, 1984.
(33) Alden, R.; Islampour, R.; Ma, H.; Villaeys, A. A. In *Density Matrix Method and Femtosecond Processes*; Lin, S. H., Ed.; World Scientific: Singapore, 1991.
(34) Harshbarger, W. R. *J. Chem. Phys.* **1970**, *53*, 903.
(35) Ågren, H.; Reineck, I.; Veenhuisen, H.; Maripuu, R.; Arneberg, R.; Karlsson, L. *Mol. Phys.* **1982**, *45*, 477.
(36) Benedict, W. S.; Plyer, E. K. *Can. J. Phys.* **1957**, *35*, 1235.
(37) Ziegler, L. D.; Hudson, B. *J. Phys. Chem.* **1984**, *88*, 1110.
(38) Ziegler, L. D. *J. Chem. Phys.* **1985**, *82*, 664.
(39) Bach, A.; Hutchison, J. M.; Holiday, R. J.; Crim, F. F. *J. Chem. Phys.* **2002**, *116*, 9315.
(40) Durmaz, S.; Murrell, J. N.; Taylor, J. M.; Suffolk, R. *Mol. Phys.* **1970**, *19*, 533.
(41) Avouris, P.; Rossi, A. R.; Albrecht, A. C. *J. Chem. Phys.* **1981**, *74*, 5516.
(42) Rosmus, P.; Botschwina, P.; Werner, H. J.; Vaida, V.; Engelking, P. C.; McCarthy, M. I. *J. Chem. Phys.* **1987**, *86*, 6677.
(43) Tang, S. L.; Imre, D. G. *Chem. Phys. Lett.* **1988**, *144*, 6.
(44) Tang, S. L.; Imre, D. G.; Tannor, D. *J. Chem. Phys.* **1990**, *92*, 5919.
(45) Dräbenstedt, A.; Fleury, L.; Tietz, C.; Jelezko, F;. Kilin, S.; Nizovtzev, A.; Wrachtrup, J. *Phys. Rev. B* **1999**, *60*, 11503.
(46) Schrand, A. M.; Huang, H.; Carlson, C.; Schlager, J. J.; Ōsawa, E.; Hussain, S. M.; Dai, L. *J. Phys. Chem. B* **2007**, *111*, 2.
(47) Loubser, J. H. N.; van Wyk, J. A. *Rep. Prog. Phys.* **1978**, *41*, 1201.
(48) Redman, D. A.; Brown, S.; Sands, R. H.; Rand, S. C. *Phys. Rev. Lett.* **1991**, *67*, 3420.
(49) Lenef, A.; Brown, S. W.; Redman, D. A.; Rand, S. C.; Shigley, J.; Fritsch, E. *Phys. Rev. B* **1996**, *53*, 13427.
(50) Collins, A. T.; Thomaz, M. F.; Jorge, M. I. B. *J. Phys. C* **1983**, *16*, 2177.
(51) Mita, Y. *Phys. Rev. B* **1996**, *53*, 11360.
(52) Gaebel, T.; Domhan, M.; Wittmann, C.; Popa, I.; Jelezko, F.; Rabeau, J.; Greentree, A.; Prawer, S.; Trajkov, E.; Hemmer, P. R.; Wrachtrup, J. *Appl. Phys. B* **2006**, *82*, 243.
(53) Zaitsev, A. M. *Optical Properties of Diamond*; Springer-Verlag: Berlin, 2001; Chapter 5.
(54) Manson, N. B.; McMurtrie, R. L. *J. Lumin.* **2007**, *127*, 98.